



## HF radar observations of small-scale surface current variability in the Straits of Florida

A. B. Parks,<sup>1,2</sup> L. K. Shay,<sup>1</sup> W. E. Johns,<sup>1</sup> J. Martinez-Pedraja,<sup>1</sup> and K.-W. Gurgel<sup>3</sup>

Received 17 July 2008; revised 11 May 2009; accepted 22 May 2009; published 5 August 2009.

[1] A dual-station high-frequency Wellen radar (WERA), transmitting at 16.045 MHz, was deployed along the eastern Florida Shelf and operated and maintained by the University of Miami's Rosenstiel School of Marine and Atmospheric Science. From September 2004 to June 2005, a moored acoustic Doppler current profiler (ADCP) acquired subsurface current measurements within the radar footprint along the shelf break at 86-m depth. The shallowest ADCP bin located at 14-m depth was used as a comparison for the WERA surface measurements. RMS differences ranged from 0.1 to 0.3 m s<sup>-1</sup> between the surface and 14-m depth, with good agreement over most of the period. Regression analyses indicated slopes near unity in the north-south ( $v$ ) component and  $\approx 0.5$  for the east-west ( $u$ ) component velocities. When utilized in tandem with the ADCP subsurface measurements, WERA enables three-dimensional snapshots of coastal oceanographic features to be resolved. For example, from December 2004 through February 2005, three energetic circulation patterns were observed: (1) a subsurface stratified countercurrent, (2) a submesoscale coherent vortex, and (3) a mesoscale circulation feature, i.e., a propagating Tortugas gyre. These features represent the significant current variability along the western flank of the Florida Current that impacts the coastal ocean.

**Citation:** Parks, A. B., L. K. Shay, W. E. Johns, J. Martinez-Pedraja, and K.-W. Gurgel (2009), HF radar observations of small-scale surface current variability in the Straits of Florida, *J. Geophys. Res.*, 114, C08002, doi:10.1029/2008JC005025.

### 1. Introduction

[2] While considerable research has been conducted in furthering our knowledge of ocean currents over basin scales, smaller-scale variability associated with coastal currents and marginal seas are not well understood. Additional complexities occur where coastal oceans are influenced by offshore western boundary currents and eddies (including small-scale coherent vortices). The difficulty in understanding the kinematical and dynamical ocean structure in coastal regions is due to the spectrum of forcing mechanisms occurring with differing temporal and spatial variability. In addition, the ocean response to these mechanisms is further complicated by the coastal geometry and bottom topographical changes.

[3] HF radar has been gaining recognition as an efficient and effective method of measuring surface currents of high temporal and spatial resolution in coastal regions. The technique of using HF radar echoes to estimate both surface wave heights and surface currents has been evolving for the past several decades on the basis of the pioneering work of

Crombie [1955]. In the HF band, the radar operates on the principle of Bragg scattering. The transmitted radar wave is backscattered by resonant surface gravity waves or "Bragg" waves that are one-half the incident radar wavelength. In the absence of a surface current, the Doppler spectrum of the returns has two peaks at the Bragg frequency ( $\nu$ ) centered around frequency zero offset by an amount proportional to  $2c_o\lambda^{-1}$ , where  $c_o$  represents the linear phase speed of the surface wave and  $\lambda$  is the radar wavelength. In the presence of an underlying current, first-order returns are Doppler shifted from the Bragg frequency by an amount  $\Delta\nu = 2V_{cr}\lambda^{-1}$ , where  $V_{cr}$  is the radial component along the radar's "look" direction. Transmissions from two separate radar sites are necessary to calculate two-dimensional surface current vectors with a prescribed Geometric Dilution of Precision (GDOP) [Chapman *et al.*, 1997]. The separation distance between the two sites determine the domain of the surface current vector images. These radar-based measurements have compared well with proven current measuring techniques such as Velocity Measuring Current Meters (VMCMs) and acoustic Doppler current profilers (ADCPs) with root-mean-square errors (RMS) of about 7 cm s<sup>-1</sup> over a range of current of 1 m s<sup>-1</sup> [Chapman *et al.*, 1997; Shay *et al.*, 1998].

[4] The Florida Current (FC) in the Straits of Florida (SOF) is an oceanic regime characterized by large horizontal current shears, relative vorticities that are up to five times the local Coriolis parameter and strong topographical gradients [Peters *et al.*, 2002]. The SOF is a narrow channel

<sup>1</sup>Division of Meteorology and Physical Oceanography, Rosenstiel School of Marine and Atmospheric Science, University of Miami, Miami, Florida, USA.

<sup>2</sup>Now at Integral Consulting, Inc., Berlin, Maryland, USA.

<sup>3</sup>Institute of Oceanography, Center for Marine and Climate Research, University of Hamburg, Hamburg, Germany.

between the southern Florida peninsula and Cuba. Given its proximity to major population centers along the eastern seaboard of the United States, the circulation in this region has been extensively studied. Notwithstanding, a common thread in all of these studies is the predominance of the FC, which connects the Loop Current (LC) in the Gulf of Mexico (GOM) to the Gulf Stream (GS) in the South Atlantic Bight (SAB). In recent years, the focus has been targeted at understanding the transient FC features such as eddies and intrusions owing to the important role they play in the biological realm and the health of coral reefs. *Lee et al.* [1995] discussed cyclonic frontal eddies near Dry Tortugas that periodically move into the Straits and translate eastward along the Keys. *Fratantoni et al.* [1998] used satellite imagery to conclude that these Tortugas gyres are the downstream expression of LC frontal eddies. As these “spin-off” eddies propagate through the southern extent of the SOF they can produce large southward displacements or meanders of the eastward flowing FC axis [*Lee et al.*, 1995; *Fratantoni et al.*, 1998; *Hamilton et al.*, 2005]. These eddies are advected in the southern SOF at approximately 5 to 15 km d<sup>-1</sup> and the coincident meanders in the FC continue to travel downstream in phase with the eddies [*Lee et al.*, 1992; *Fratantoni et al.*, 1998].

[5] *Shay et al.* [1998] utilized land-based ocean surface current radar (OSCR) to observe a submesoscale vortex progressing eastward at 30 cm s<sup>-1</sup>. Given its dipole-like structure, this event had a horizontal scale of 40 km but was unlike the spin-off eddies forced by frontal disturbances as discussed by *Lee and Mayer* [1977] in that the signal was absent in the subinertial band defined as 48-h low-pass signals. The feature was embedded in the near-inertial passband and may have been generated by an abrupt change in wind direction and stress over the shelf consistent with wind-forced near-inertial wave dynamics [*Kundu*, 1976a]. *Shay et al.* [2000] observed complex surface circulations including submesoscale vortices over the shelf break at Ft. Lauderdale, FL using OSCR in very high frequency (VHF) mode. Measurements were acquired at 20-min intervals at a spatial resolution of 250 m [*Shay et al.*, 2002]. One coherent vortex observed during this experiment had a similar translation speed of approximately 30 cm s<sup>-1</sup>, with a horizontal extent of only 2 to 4 km. Interestingly, winds were relatively calm throughout the experiment. In OSCR field experiments deployed during the summer and winter of 1998, numerous small-scale eddies were observed in the velocity record, some of which were FC spin-off-type eddies [*Haus et al.*, 2000, 2004]. The eddy spatial scale varied between the summer and winter months. However, the study duration was insufficient to ascertain the role of seasonal wind forcing, local topography and other factors on these observations. In this context, more detailed current observations with depth are needed to gain insight into the structure of these features and their forcing mechanisms. Advantages from combining WERA surface currents and subsurface ADCP measurements have been shown by *Liu et al.* [2007] along the West Florida Shelf. These data sets exhibited three-dimensional, time-dependent current structures which are distinct for differing processes in this region (i.e., tides, near-inertial motions, and weather-induced variability). This result would not have been possible using one measurement technique alone.

[6] As part of the ONR-sponsored Southeast Atlantic Coastal Ocean Observing System (SEA-COOS), a high-frequency (HF) Wellen radar system (WERA) is currently operated and maintained by the University of Miami's Rosenstiel School of Marine and Atmospheric Science along the eastern Florida Shelf (EFS). The surface current data observed using this technology contains a broad spectrum of temporal and spatial variability due in part to energetic and coherent small-scale coastal ocean processes [*Shay et al.*, 2008]. Concurrent ADCP measurements acquired within the radar footprint provide a detailed view of the kinematical structure of these features. A comparison between the WERA and ADCP measurements was conducted over the 9-month deployment period for the ADCP. East-west (*u*) and north-south (*v*) component velocities from hourly averaged WERA measurements are compared to subsurface velocity components from the 14-m surface most bin of the ADCP. This analysis includes estimation of root-mean-square (RMS) differences, means and standard deviations. Time series from WERA-derived surface current measurements and concurrent measurements from the ADCP were then analyzed to investigate energetic features. Events were selected from the record to examine the kinematical structure and variability of particular surface circulation patterns. These patterns include submesoscale circulation features, FC meander events and periods of decorrelation between the WERA surface currents and ADCP subsurface currents. In this framework, the experimental design is described in section 2 with measurements given in section 2. In section 3, vector surface and subsurface currents are compared from September 2004 to June 2005. Three interesting events occurring from December 2004 through February 2005 are documented in section 4. A summary and concluding remarks are given in section 5.

## 2. Measurement and Experimental Design

[7] In June 2004, two WERA stations were deployed along the EFS between Key Biscayne, FL and Key Largo, FL. During this period of operation, an ADCP was deployed within the radar footprint from September 2004 to June 2005 [*Gurgel et al.*, 1999a; *Shay et al.*, 2007]. In this section, the experimental design including WERA system, ADCP mooring specifications and a National Data Buoy Center (NDBC) Coastal Marine Automated Network (C-MAN) station are described.

### 2.1. WERA Characteristics

[8] WERA transmits a frequency modulated continuous wave (FMCW) chirp at 0.26 sec intervals and avoids the blind range of interrupted FMCW in front of the radar [*Gurgel et al.*, 1999b; *Essen et al.*, 2000; *Shay et al.*, 2007]. The range of frequencies used for WERA is from 3 to 30 MHz with more common transmission frequencies of 8 and 16 MHz corresponding to Bragg wavelengths of 18.8 and 9.4 m, respectively (Table 1). At a transmission frequency of 16.045Hz, WERA system requires 126-m baseline distance for a 16-element phased array to achieve a narrow beam electronically steered over the illuminated ocean footprint. Beam width is a function of the radar wavelength divided by the length of a phased array, which is 7.5° for the 16-element phased array. The transmitter is

**Table 1.** Capabilities of the 16 MHz WERA System

	Value
Operation range (km from radar site)	80
Range cell resolution (km)	1
Measurement depth (m)	0.7
Measurement cycle (min)	<10
Radial current accuracy ( $\text{cm s}^{-1}$ )	1.8
Vector current accuracy ( $\text{cm s}^{-1}$ )	$\text{GDOP} \times \text{RCA}$
Beam width at 16 antennae (deg)	$\pm 3$
Bragg wavelength (m)	9.4
Transmit elements (phased array)	4
Receive elements (BF)	8–16
Receive elements (DF)	4
Transmit power (W)	30

arranged to encompass a  $120^\circ$  swath. WERA has the flexibility to be configured in direction-finding (DF) mode (such as Coastal Ocean Dynamics Application Radar (CODAR)) where 4 receive antennae are set up in a square array, or in beam-forming (BF) mode from a linear array consisting of  $4n$  (where  $n = 2, 3,$  and  $4$ ) elements or channels. As the number of receiver antennae elements increase, current vector resolution improves [Teague *et al.*, 2001]. A medium-range, high–horizontal resolution version was designed with a range of  $\approx 80$  km with horizontal resolution of 1.2 km depending on the available bandwidth approved by the Federal Communication Commission. Higher spatial resolution requires bandwidth of more than 200 kHz (i.e.,  $\pm 100$  kHz). Temporal sampling can be as low as a few minutes since the WERA system is FMCW. This sampling feature is attractive for high-current regimes such as the FC where time scales of variability associated with large horizontal shear vorticities are less than an hour [Peters *et al.*, 2002].

## 2.2. EFS Experimental Design

[9] The EFS radar network consists of two WERAs that provide near–real time surface currents to SEA-COOS and the Internet [Gurgel *et al.*, 1999a; Shay *et al.*, 2007, 2008]. In its fifth continuous year of operation, the radars are located at

Crandon Park on Key Biscayne ( $25^\circ 42.84'N, 80^\circ 9.06'W$ ) and Key Largo ( $25^\circ 14.46'N, 80^\circ 18.48'W$ ) Florida. Each site contains 4 transmitting antennae (Tx) and 16 receiving antennae (Rx). Figure 1 shows approximate radar coverage for this WERA system. Operating at a frequency of 16.045 MHz, the radar maps surface currents every 20 min over approximately 5000 cells with a cell resolution of  $\approx 1.2$  km (higher resolution is possible with more bandwidth). Receiver and transmitter cables are calibrated to monitor any variations in signal amplitudes and phases.

## 2.3. Radial Current

[10] As shown in previous studies, the frequency shift off the Bragg frequency due to Bragg resonant waves traveling along a nonmoving ocean surface is proportional to the radial current [Crombie, 1955; Stewart and Joy, 1974]. Both positive and negative Doppler shifts can be observed because of advancing (positive) or receding (negative) waves, and this frequency utilizes the Doppler spectral peak. For the 16.045 MHz system used here, the corresponding Bragg frequency is 0.409 Hz.

[11] Accuracy of the radial current is estimated from the statistics of the velocities within a given grid cell (K.-W. Gurgel, personal communication, 2006). Briefly, for each  $n$  sample interval in time, radial current accuracy is estimated by accounting for signal strength (SNR) as well as horizontal shear within a grid cell. The magnitude of the radial current accuracy is combined through the sum of the squares from each snapshot then time averaged over the grid point given by

$$r_{acc} = r_\sigma \sqrt{n^{-1}}, \quad (1)$$

where  $r_\sigma^2 = \frac{\sum_{i=1}^n r^2(i) \text{SNR}(i)}{\sum_{i=1}^n \text{SNR}(i)} - \bar{r}^2$  and  $\bar{r} = \frac{\sum_{i=1}^n r(i) \text{SNR}(i)}{\sum_{i=1}^n \text{SNR}(i)}$ ,  $n$  is the number of samples of  $r(i)$  from the Bragg peak in the BF mode. In this approach of accuracy, the SNR is used as a

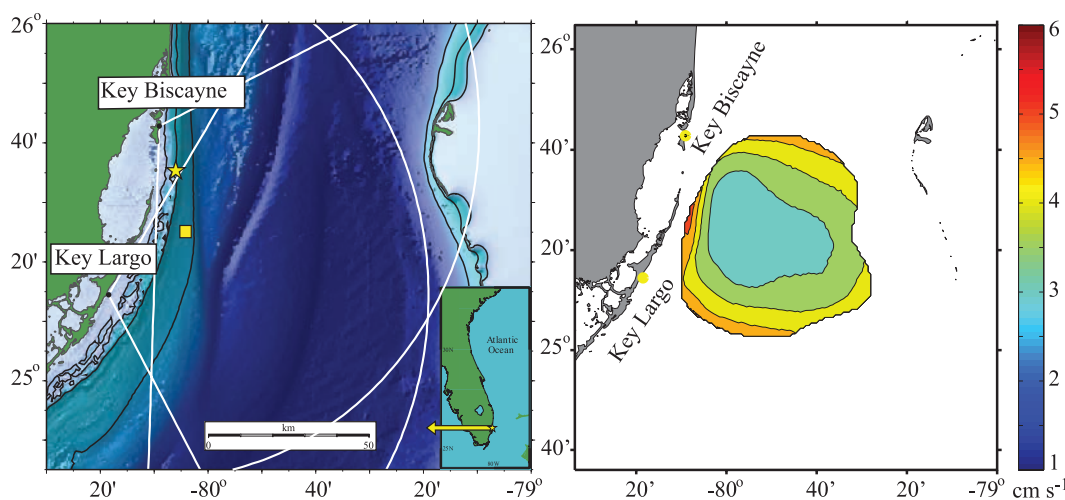


**Figure 1.** (left) Map of WERA deployment along SE Florida with depth in color contours. The white arcs represent the  $120^\circ$  swath which is covered by the WERA transmission. Backscatter is collected on a 1.2-km grid every 10 min from alternating sites. The yellow star refers to the location of Fowey Rocks C-MAN station maintained by the National Data Buoy Center. The yellow square refers to the location of the ADCP mooring (water depth is 86 m at the mooring site). (right) Mean radial accuracy within domain receiving data with radial accuracies of  $10 \text{ cm s}^{-1}$  or better more than 70% of the study duration.

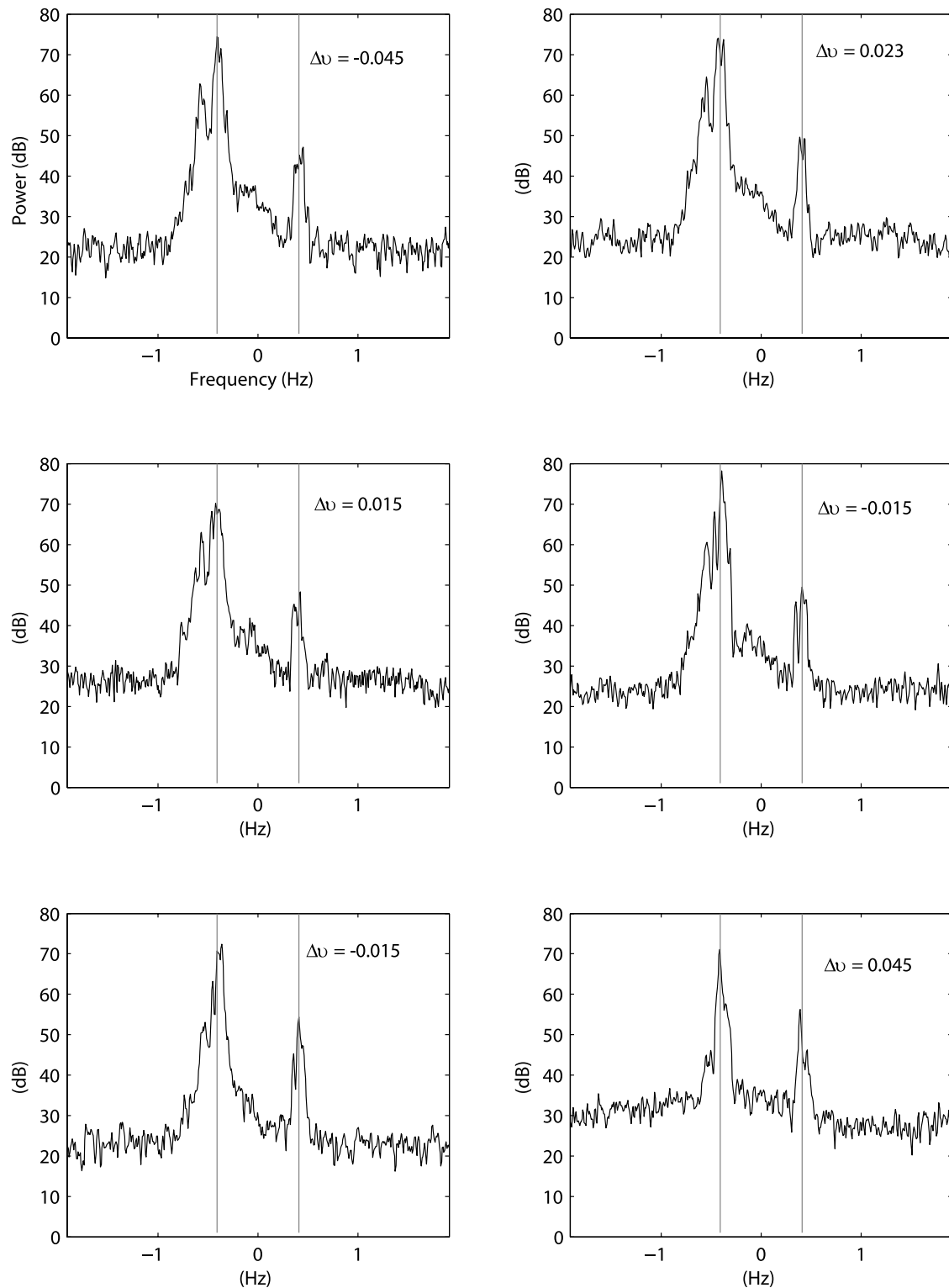


**Figure 2.** Doppler spectra shown for 3-h periods between 0600 and 2100 GMT on 20 January 2005. Distinguishable Bragg peaks allow for computation of  $\Delta\nu$  from which radial currents are derived.

weighting function that provides a better estimate of the accuracy [Shay *et al.*, 2007]. A similar approach can be used for DF mode of HF radars. Generally, higher data accuracy are obtained close to the coast as signal strength attenuates seaward away from the radar sites. The range of ground wave signals is a function of transmitter frequency, seawater

conductivity and atmospheric conditions [Broche *et al.*, 1987; Gurgel *et al.*, 1999a, 1999b]. In the present application, the magnitude of the radial current accuracy is combined through the sum of the squares from each sample ( $r_{oc}^2 + r_{ot}^2$ ) from Crandon and Key Largo then time averaged over the appropriate intervals. During the course

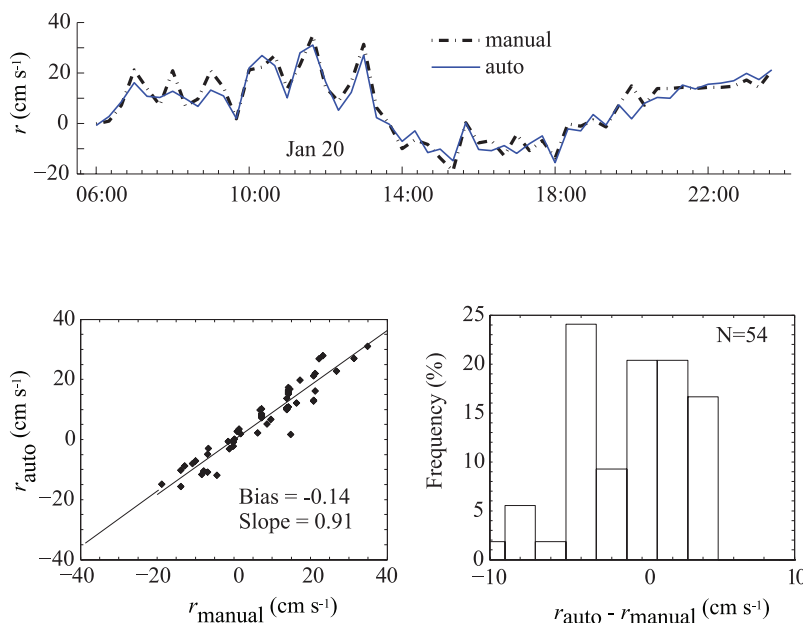


**Figure 3.** (top) Twenty-minute time series of manually calculated,  $r_{manual}$ , and automated,  $r_{auto}$ , radial currents from 0600 to 2340 GMT, 20 January 2005 in  $\text{cm s}^{-1}$ . (bottom left) Scatter of  $r_{manual}$  and  $r_{auto}$  ( $\text{cm s}^{-1}$ ). (bottom right) Histogram of manual and automated radial differences indicates that error in the measurements will not significantly impact calculations based on these velocity fields.

of the experiment, a  $60 \text{ km} \times 60 \text{ km}$  portion of the domain has yielded data returns with less than  $6 \text{ cm s}^{-1}$  radial current accuracies greater than 70% of the time. Radial accuracy is shown (Figure 1) over the ADCP deployment period within this region. Given the SNR values, radial current accuracy ranged from  $3$  to  $5 \text{ cm s}^{-1}$ , suggestive of quality surface current measurements in a highly dynamic regime such as the Florida Current.

[12] To exhibit the capability of WERA to resolve currents across the shear zone of the FC, Doppler spectra from an individual cell along the shelf break are shown in Figure 2. These data were observed during a pronounced submesoscale event on 20 January 2005 [Parks, 2008]. Bragg peaks are clearly identifiable allowing for accurate estimation of  $\Delta\nu$  or the frequency shift off of the Bragg frequency in the spectra. However, notice that the spectral peaks are broader and there are “double” peaks in the spectra because of the strong horizontal velocity shears in this regime. Similar behavior was found previously in HF radar measurements acquired across the Gulf Stream [Shay *et al.*, 1995] and FC [Shay *et al.*, 1998]. To examine the relative differences between the automated procedure versus manually calculated values, the time series of the corresponding radial currents is shown in Figure 3. In general, there are less than  $4 \text{ cm s}^{-1}$  differences between the two approaches where the scatter from radial currents are well behaved in relation to the regression line with a small bias. These differences will have a minimum impact on shear estimates across the FC front.

#### 2.4. Vector Current and Its Accuracy

[13] Two radial components of the surface current are combined to give the total vector current at each grid cell. The cartesian current components are a function of the bearing angles relative to the radar bore sites from the Key Largo and Key Biscayne radar sites as in other venues.

Critical to creating reliable vector current fields from HF radar radial measurements is the intersection angle between the radials emanating from each site. Phased array geometrical limitations are set by the angle of the phased array along the coastline [Gurgel, 1994]. In this HF radar domain, acceptable angles of intersection, defined as  $30^\circ \leq \alpha \leq 150^\circ$ , occurred throughout the region except for cells located closest to shore and in the far northeast and southeast corners of the domain (i.e., in close proximity to the Bahama Bank). These outer limits were beyond the maximum range ( $\approx 80 \text{ km}$ ) of the radar stations. This influence of the geometry on the measurement errors (GDOP) is well known from the Global Positioning System (GPS) and is a factor describing the increase or decrease of the total error due to geometry. On the basis of the Chapman *et al.* [1997] algorithm, the GDOP in this domain ranges from 1 to 2.5. In the core of the domain, GDOP values are less than 1.5. In the far field of the radar ( $\approx 80 \text{ km}$ ), these values are greater than 2 where the current intersection angles approached  $30^\circ$ . The EFS WERA network has been operational more than 92% of the time since its initial deployment in June 2004 (see Figure 4). Shay *et al.* [2008] discuss lessons learned using HF radars in the Southeast and Gulf of Mexico where land-falling hurricanes impact operations.

#### 2.5. Moored ADCP

[14] A bottom-mounted, upward-looking ADCP (manufactured by RD Instruments (RDI)) operating at  $300 \text{ kHz}$  was deployed offshore of Elliott Key at approximately  $86\text{-m}$  depth. This instrument was located at  $25^\circ 24.04'\text{N}$ ,  $80^\circ 5.9'\text{W}$ , a position inside the HF radar domain approximately  $0.55 \text{ km}$  from the nearest cell, over a 9-month period from September 2004 to June 2005. Ensemble averaging of the backscattered acoustic signals formed a time series at  $2\text{-m}$

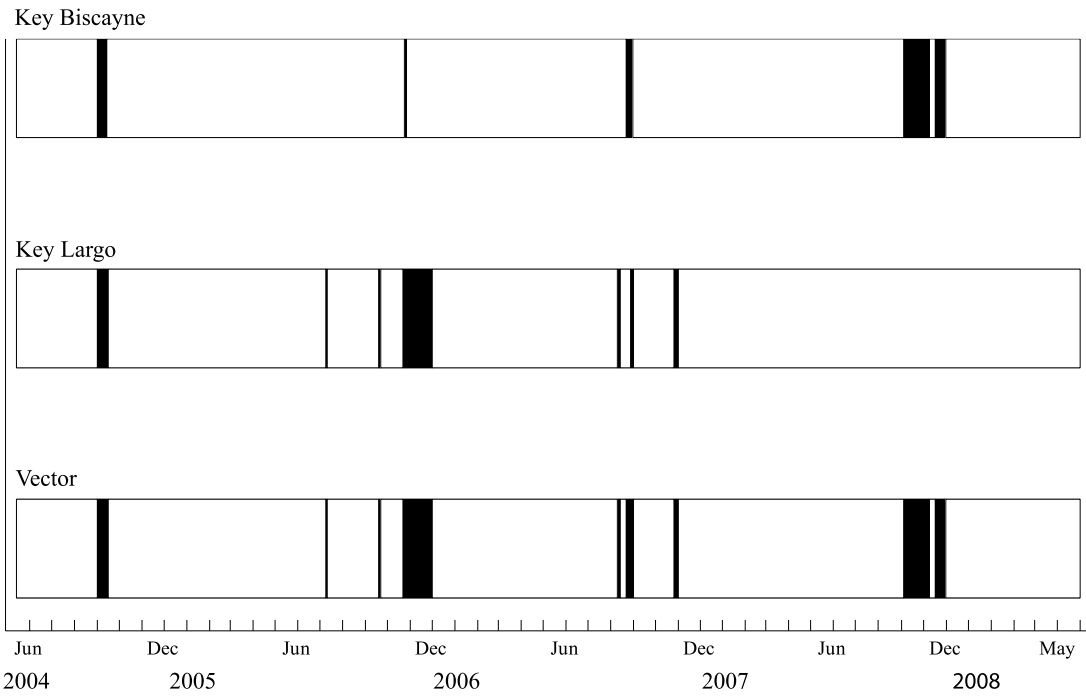


**Figure 4.** Black lines indicate inoperable time periods at sites (top) Key Biscayne and (middle) Key Largo and (bottom) combined vector data from June 2004 through June 2008.

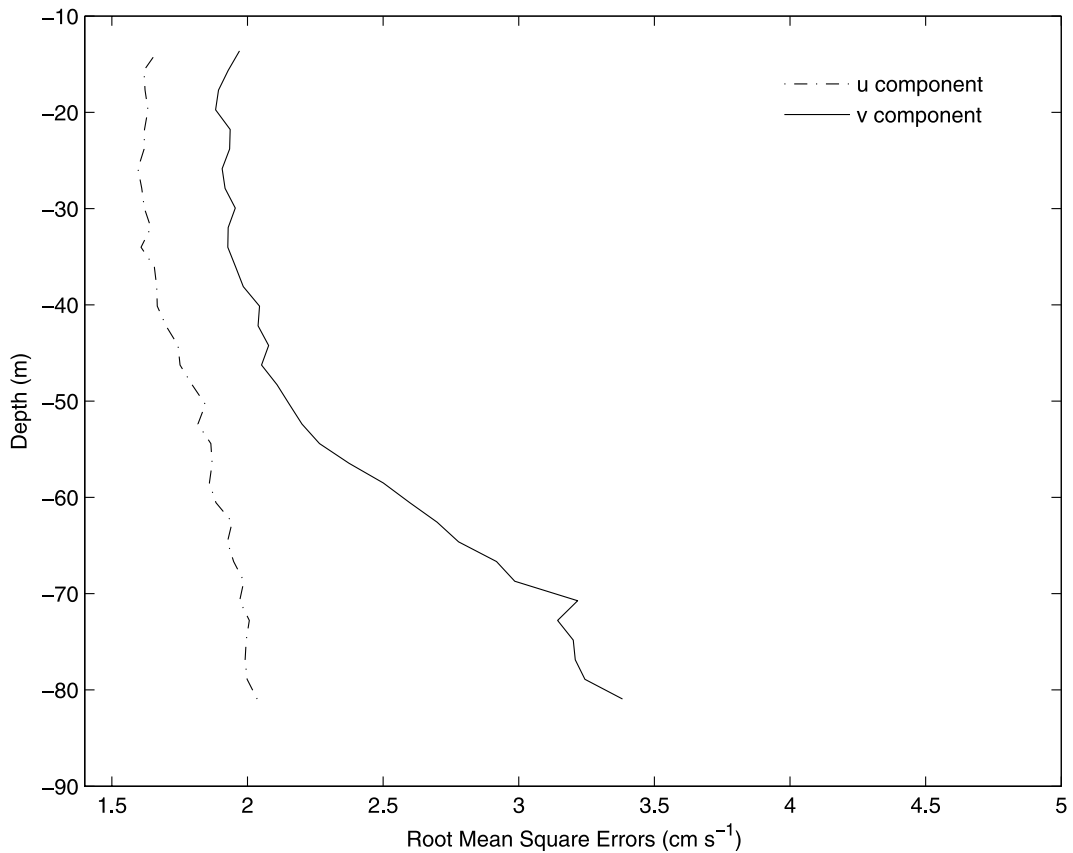


**Figure 5.** Bin-bin root-mean-square error differences for the north-south (*v*, solid) and east-west (*u*, dash-dotted) velocity components average over the entire ADCP deployment.

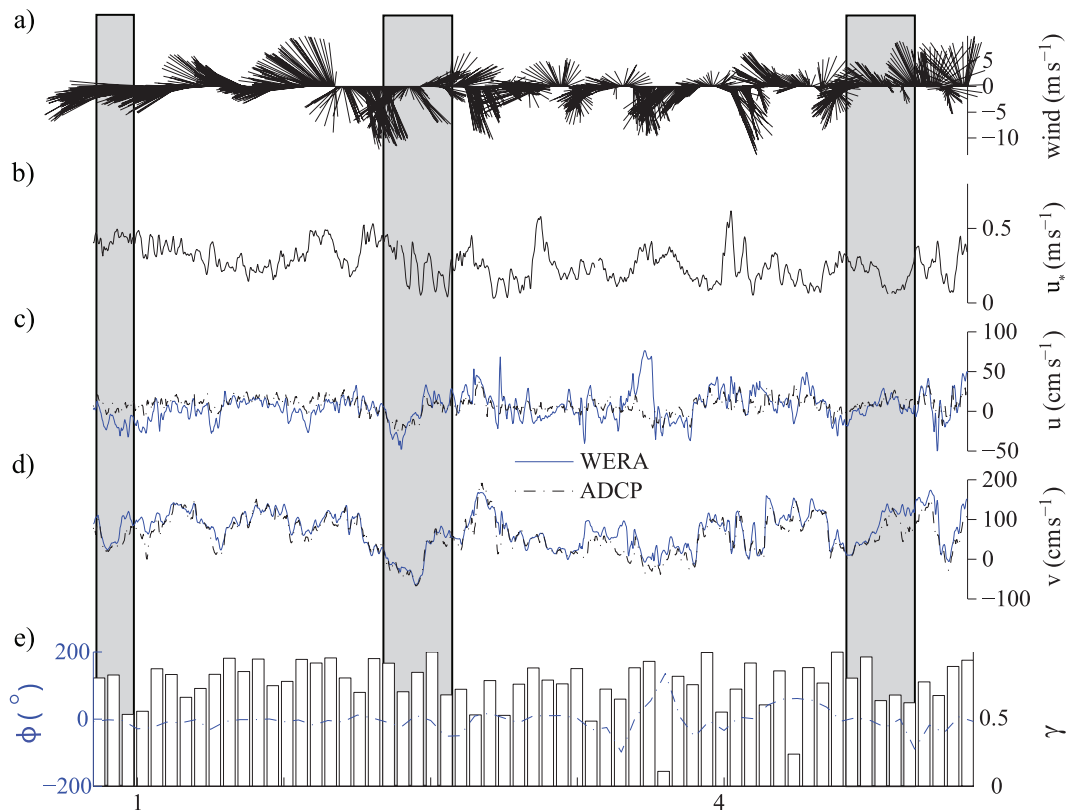


**Figure 6.** Time series analysis from 28 December 2004 through 28 February 2005: (a) 3-point Hanning windowed wind vectors ( $\text{m s}^{-1}$ ) from Fowey Rocks C-MAN station rotated into an oceanographic context, (b) surface frictional velocity ( $u_*$  ( $\text{m s}^{-1}$ )) from Fowey Rocks based on the work by *Fairall et al.* [1996], and corresponding time series comparison of (c) cross-shelf ( $u$ ) and (d) along-shelf ( $v$ ) components ( $\text{cm s}^{-1}$ ) for the surface (blue) and 14-m subsurface currents (black) using 3-point Hanning windowed data subsampled at hourly intervals. (e) Daily averaged complex correlation coefficients (bars) and phase angle (blue dash-dotted line). Gray shading marks the times of events discussed in this paper.

vertical intervals at 30-min temporal intervals from the surface to the bottom. Errors commonly occur in bottom-mounted ADCP measurements near the surface because of sidelobe interference. Current signals from near-surface bins were analyzed for noise interference over the 9-month record. Consequently, the bin at 14-m depth was utilized as the surface most bin not susceptible to contamination by sidelobe returns. This assures that high-quality samples are used for the comparison, but it does not necessarily mean that surface currents are being compared to ocean mixed layer currents. The closest cell, located at  $25^\circ 23.85' \text{N}$  and  $80^\circ 5.7' \text{W}$ , is used in this analysis. To facilitate direct comparison of the ADCP-derived current measurements to the hourly averaged surface currents, ADCP data were first windowed using a three-point Hanning window [*Otnes and Enochson, 1978*] and subsampled at hourly intervals. Prior to comparing  $u$  and  $v$  currents, bin-to-bin root-mean-square (RMS) differences were estimated for the ADCP over the 9-month deployment period (Figure 5). RMS differences were less than  $2 \text{ cm s}^{-1}$  in the upper 50 m of the water column for the  $u$  and  $v$  components.

## 2.6. Local Winds

[15] Hourly wind speed and direction measurements from September 2004 to June 2005 were obtained from the NDBC C-MAN station located at Fowey Rocks ( $25^\circ$

$35.4' \text{N}$ ,  $80^\circ 6.0' \text{W}$ ), just inshore of the WERA radar domain. Wind magnitude and direction data were converted to the 10-m reference level [*Large and Pond, 1981*]. Subsequently, these data were transformed to  $u$  and  $v$  component velocities in an oceanographic context and also smoothed using a three-point Hanning window [*Otnes and Enochson, 1978*]. Wind stress ( $\tau$ ) components and the surface frictional velocities ( $u_*$ ) were calculated using adjusted 10-m measurements following *Fairall et al.* [1996]. These results are plotted over monthly time scales and aid in depicting the effects of varying surface stress on the  $u$  and  $v$  component velocity correlation between the ocean surface currents and 14 m depth (Figure 6).

## 3. Comparisons

### 3.1. Time Series

[16] Considering the general agreement of the concurrent data sets throughout the time series, a comparison is documented herein to understand both correlated and decorrelated periods, the latter case being of more interest. Initially, both data sets were quality controlled by analyzing the time series in 1-month segments. Data values more than two standard deviations from the mean were removed from the time series and replaced by a linear interpolation for gaps of a few-hours duration. Large gaps (e.g., power grid

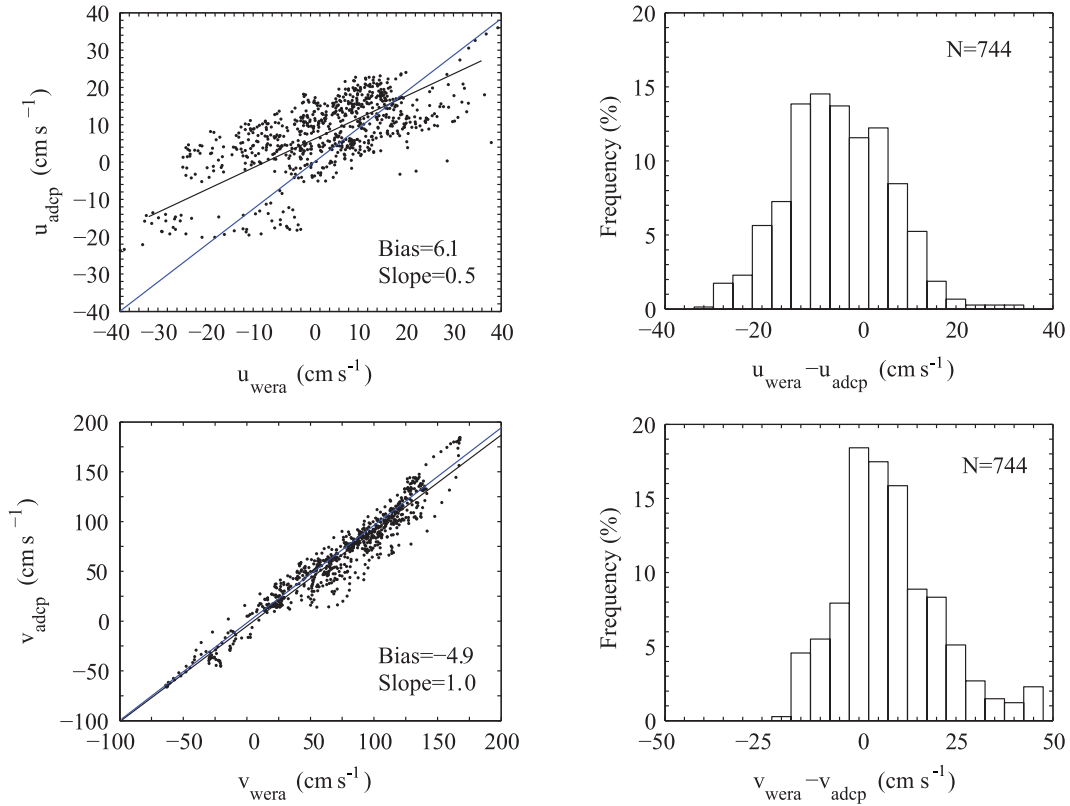


**Figure 7.** Scatter diagrams ((top left)  $u$  and (bottom left)  $v$ ) and histograms ((top right)  $u$  and (bottom right)  $v$ ) from the month of January 2005. WERA surface current data are shown along the  $x$  axis, and ADCP data from the 14-m bin are along the  $y$  axis. Thicker, black lines represent ideal slope. Slopes for the  $u$  and  $v$  scatters are 0.45 and approximately 1, respectively.

shutdown) were not included in this analysis. One statistical measure of the correlation between two differing vector measurements is the complex correlation coefficient and phase angle [Kundu, 1976b]:

$$\gamma = \frac{\langle u_o u_{14} + v_o v_{14} \rangle + i \langle u_o v_{14} - v_o u_{14} \rangle}{\langle u_o^2 + v_o^2 \rangle^{1/2} \langle u_{14}^2 + v_{14}^2 \rangle^{1/2}} \quad (2)$$

$$\phi = \tan^{-1} \frac{\langle u_o v_{14} - v_o u_{14} \rangle}{\langle u_o u_{14} + v_o v_{14} \rangle}, \quad (3)$$

where  $u$  and  $v$  represent cross- and along-shelf current components and subscripts  $o$  and  $14$  denote surface current

data and subsurface (14-m depth) measurements from the ADCP, respectively. This phase angle represents the average cyclonic angle of the subsurface current vector with respect to the surface current vector. Correlation coefficient and phase angle were calculated and plotted throughout the ADCP deployment (see Figure 6e). Typical values for complex correlation coefficient were greater than 0.8 with phase angles approach zero showing consistent agreement between the two data sets separated by 14 m in depth.

### 3.2. Scatter Diagrams and Histograms

[17] Scatter diagrams and histograms for the  $u$  and  $v$  component velocities from both instruments were plotted on a monthly basis and linearly fit (e.g., Figure 7). Typical

**Table 2.** Monthly RMS, Slope, and Bias Comparison Between HF Radar-Derived Surface Currents and 14-m Subsurface ADCP Measurements<sup>a</sup>

	2004				2005					Entire Record
	Sep	Oct	Nov	Dec	Jan	Feb	Mar	Apr	May	
$u$ ( $\text{cm s}^{-1}$ )										
RMS	29.1	29.3	10.0	8.8	9.5	13.9	13.1	12.1	15.5	16.6
Slope	-0.1	0.0	0.4	0.4	0.5	0.1	0.4	0.3	0.3	0.2
Bias	7.2	15.4	11.5	10.2	5.8	7.2	6.3	8.2	12.3	11.3
$v$ ( $\text{cm s}^{-1}$ )										
RMS	13.2	10.4	14.6	14.7	12.3	22.2	29.7	22.7	24.2	18.9
Slope	1.1	1.1	0.8	0.8	1.0	0.9	0.9	0.8	1.0	0.9
Bias	-11.5	-7.7	10.6	2.8	-5.0	-12.0	-21.0	-3.3	-21.1	-8.8

<sup>a</sup>High RMS values are mainly attributed to stratification.

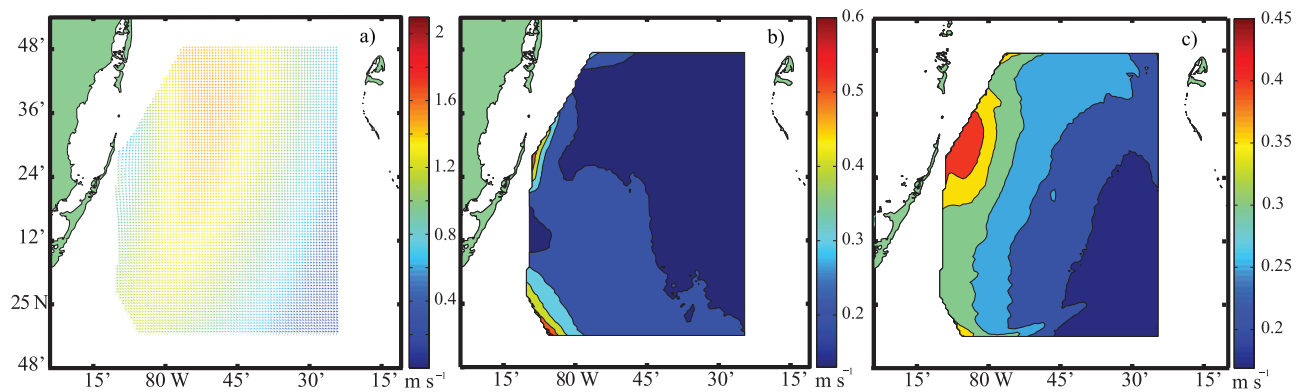


**Figure 8.** (a) Annual mean surface currents ( $\text{cm s}^{-1}$ ) from 2005 WERA HF radar measurements on a 2.4-km grid to facilitate visualization. Mean currents agree well with previous surface current observations in the FC. Annual standard deviation ( $\text{cm s}^{-1}$ ) of (b)  $u$  and (c)  $v$  components of surface current.

regression slopes for the  $v$  component were  $\approx 0.8$  to 1 over the 9-month duration. Similarly,  $u$  component slopes were  $\approx 0.4$  to 0.5 from November 2004 to January 2005 and decreased to  $\approx 0.1$  to 0.4 over other months of the deployment. These results suggest that cross-shelf motions dominate the eddy variability when the FC axis is aligned in the along-shelf (primarily north-south) direction. For example, coastal countercurrents and small-scale eddy variability in the coastal zone influence the cross-shelf component velocity. Seasonal variability associated with wind forcing exhibits a peak in winter months (excluding tropical cyclone passage during the summer months). Thus, surface and subsurface motions tend to be more correlated during the winter months.

### 3.3. Descriptive Statistics

[18] RMS differences were calculated between the surface current and 14-m subsurface data, in addition to slope

and bias, on a monthly basis and over the 9-month record (see Table 2). RMS differences ranged from 0.1 to 0.3  $\text{m s}^{-1}$  for both the  $u$  and  $v$  components between the surface and 14-m depth, consistent with previous measurements acquired off Dania Beach [Shay *et al.*, 2002]. As stated above, these cross-shelf ( $u$ ) values were much lower during the winter months when wind forcing and the resulting surface stresses induce a well-mixed upper ocean because of vertical shear.

[19] The annual mean surface current from 2005 is shown in Figure 8 with standard deviation of the  $u$  and  $v$  component velocities. Mean currents agree well with previous investigations of the FC in this region. Standard deviations in the  $u$  component increase shoreward of the 20-m isobath compared to the  $v$  component which increase shoreward of the 200-m isobath.

[20] This suggests that variability in the  $u$  component is indeed related to smaller-scale motions that impact the

**Table 3.** Monthly Mean, Standard Deviation, and Maxima and Minima for Hanning Windowed East-West and North-South Current Components From WERA Surface Current Data and the 14-m Depth From ADCP Measurements<sup>a</sup>

	2004				2005				
	Sep	Oct	Nov	Dec	Jan	Feb	Mar	Apr	May
$u^{\text{WERA}}$									
Mean	-16.7	-11.3	6.2	7.8	3.6	10.9	3.1	4.0	6.0
SD	19.8	17.9	10.0	12.4	15.4	21.5	25.3	17.5	27.8
Min	-82.2	-74.0	-28.5	-32.4	-47.8	-49.9	-110.9	-66.3	-108.2
Max	32.5	37.6	39.6	40.6	68.4	94.1	77.9	59.5	52.1
$v^{\text{WERA}}$									
Mean	57.6	78.9	104.2	98.6	73.0	75.9	83.6	84.7	101.8
SD	42.4	47.0	32.1	28.1	48.4	47.0	41.3	35.4	31.5
Min	-28.3	-41.1	27.5	22.8	-64.9	-16.5	-39.9	-63.2	-6.5
Max	140.1	197.5	189.8	165.3	168.1	173.7	215.2	173.9	154.6
$u_{14\text{m}}$									
Mean	9.3	15.3	14.6	13.5	7.7	8.8	7.4	9.3	13.9
SD	10.2	14.0	7.0	7.4	10.5	11.6	12.5	9.8	10.8
Min	-11.3	-22.5	-5.1	-6.7	-27.0	-21.1	-32.7	-35.2	-23.2
Max	37.3	55.6	40.3	33.8	40.3	50.3	56.0	28.9	52.4
$v_{14\text{m}}$									
Mean	50.7	75.6	96.1	85.3	65.1	55.1	55.7	65.6	81.5
SD	48.3	51.7	33.7	28.0	49.3	46.3	47.9	37.5	43.1
Min	-39.0	-68.6	11.6	19.1	-67.7	-38.1	-58.9	-83.7	-50.9
Max	137.4	206.5	179.9	156.6	193.6	148.7	208.2	140.3	157.1

<sup>a</sup>Note that September measurements begin at 16 September 2004 because of bad WERA data during hurricanes Frances and Jeanne in the early part of the month. Consequently, statistics for September represent only half of the month's ADCP record. Maxima and minima are in  $\text{cm s}^{-1}$ . East-west component,  $u$ ; north-south component,  $v$ .

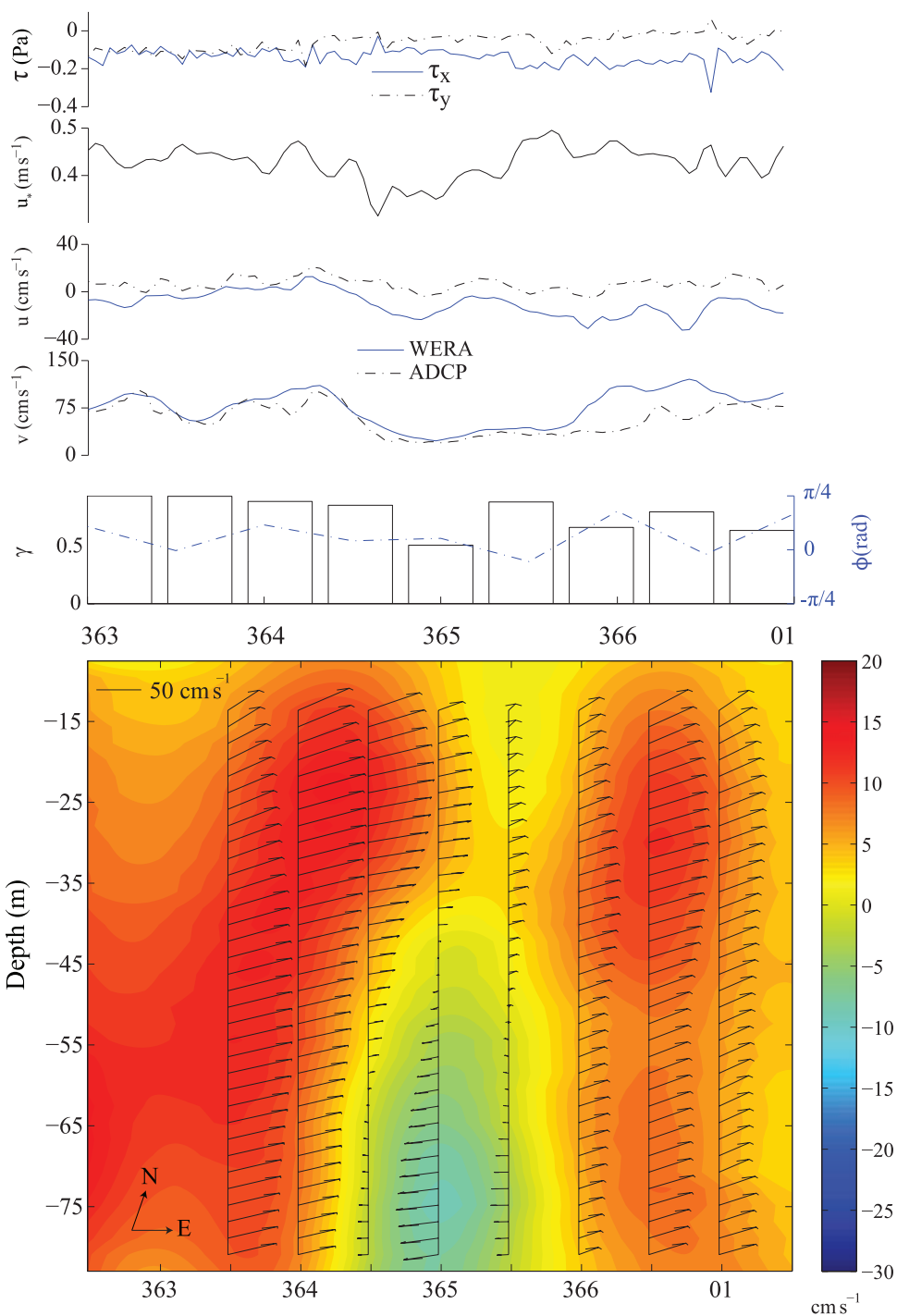


**Figure 9.** (top) Time series analysis from 28 through 31 December 2004 (YD 363–01); same as Figure 6 except with wind stress,  $\tau_x$  and  $\tau_y$ , and 3-h-averaged complex correlation coefficients (bars) and phase angle (blue dash-dotted line). (bottom) The  $u$  component velocity contours (eastward (positive)/westward (negative) in  $\text{cm s}^{-1}$ ) from 8-m to 82-m depth and current vectors ( $\text{cm s}^{-1}$ ) every 12 h from 14-m to 80-m depth during the same time period.

narrow (typically 7 to 15 km wide) shelf, however the variability in the  $v$  component is due to both submesoscale and larger mesoscale features that may extend seaward past the shelf break [Parks, 2008]. Standard deviation increases in the southward extent of the radar domain are an artifact of radial current accuracy decreases outside the 70% region (Figure 1). Means, standard deviations, and smallest- and

largest-order statistics are given in Table 3 on a monthly basis and reveal a highly variable domain dominated by the FC. For example, in the east-west direction, surface currents ( $u_o$ ) have the most eastward flowing mean velocity in February yet in March, the largest currents flow westward across the shelf. North-south surface currents ( $v_o$ ) have a range of  $2.15 \text{ m s}^{-1}$  to  $-0.65 \text{ m s}^{-1}$ , depicting the large

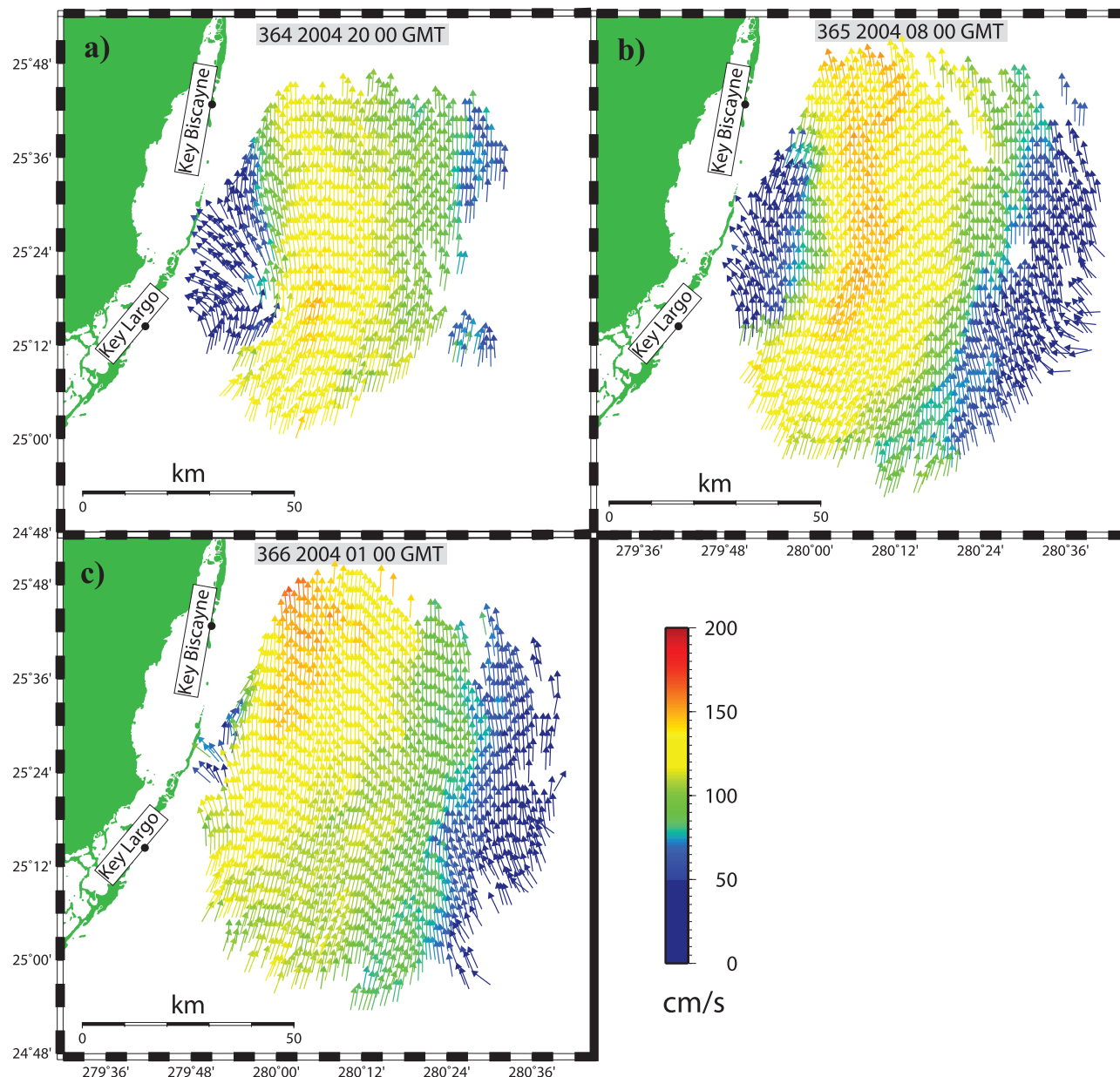


**Figure 10.** Hourly averaged WERA surface current maps on a 2.4-km grid showing frontal eddy passage inshore of the FC. (a) Frontal eddy propagates into southwestern portion of radar domain as FC is deflected offshore. (b) FC begins to shift back shoreward as frontal eddy moves north. No center of circulation is evident in WERA images during this time. (c) FC continues to return close to its mean state.

dynamical range of this energetic western boundary current. In comparison, east-west subsurface currents ( $u_{14}$ ) show dramatic differences throughout the study with much weaker flows. Of particular interest for future studies are times of flow reversals between surface and subsurface currents as observed in the time series during September and October 2004.

#### 4. Ocean Features

[21] From the analysis of monthly time series, three events from the months of December 2004 to February 2005 were selected and investigated as depicted by gray shaded area (see Figure 6). Parks [2008] documented

several eddy-like events from 2006 using HF radar derived surface currents and an approach based on Okubo-Weiss parameter maps. The analysis of the observed features in 2006 have similar characteristics to those discussed below from the concurrent radar and ADCP measurements.

##### 4.1. Subsurface Stratified Flow

[22] As shown in Figure 9, a subsurface stratified countercurrent was observed in the ADCP measurements that persisted from 29 to 31 December (YD 364–366) prior to the water column resuming a more barotropic structure. On 29 December, surface currents indicated continuity with the 14-m bin in the along-shelf component whereas the cross-shelf component velocity exhibited differences at times

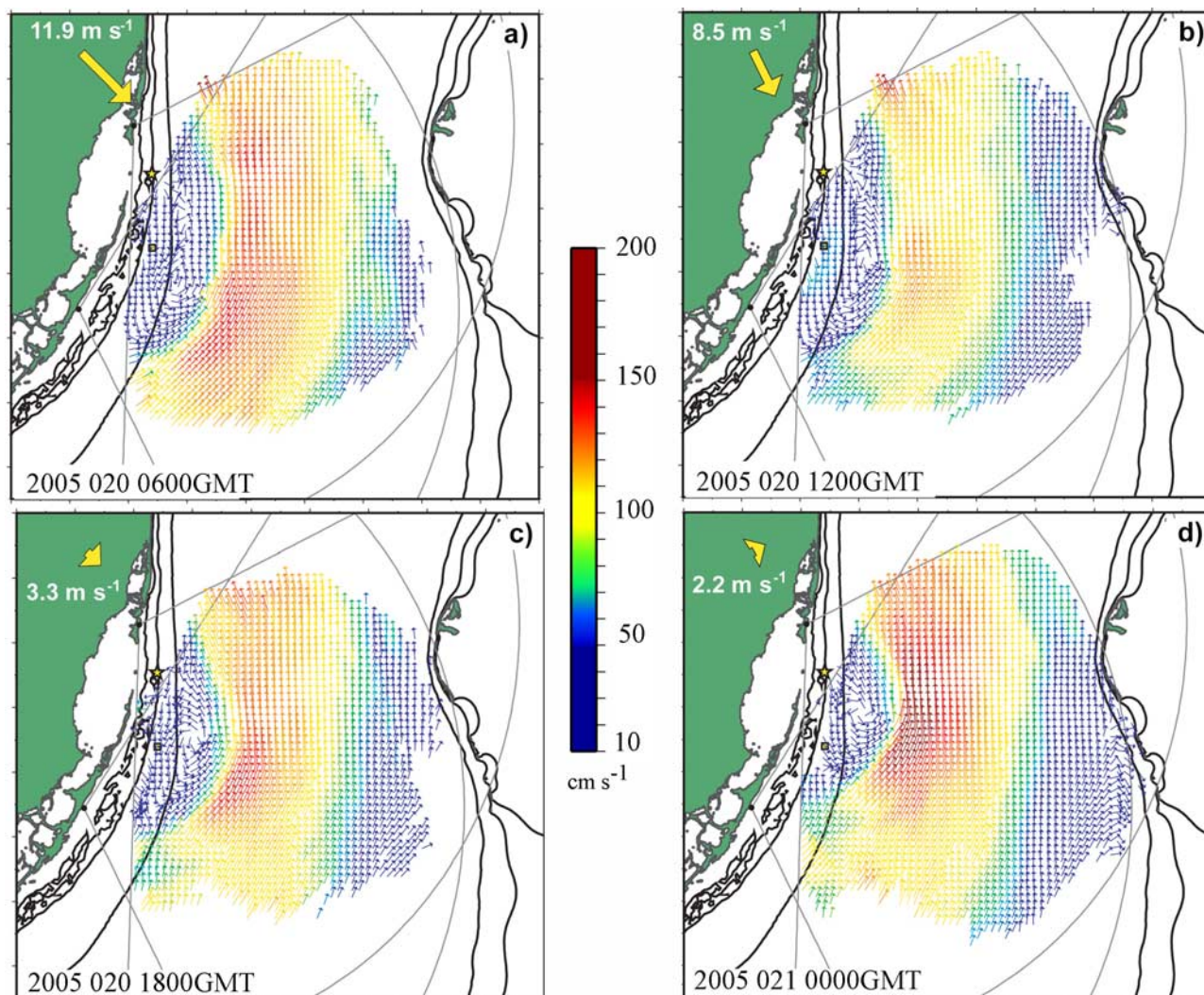


**Figure 11.** Hourly averaged WERA surface current observations on a 2.4-km grid showing a small vortex propagating northward in response to a cold front passage. Winds from Fowey Rocks (depicted by yellow star) are shown as yellow vectors in the upper left portion of image. (a) Front at its strongest; vortex centered along 200-m isobath. (b) Coastal southward flow increases as center of vortex moves north of 200-m isobath. (c) Vortex continues to move north seaward of 200-m isobath as winds associated with front subside. (d) Vortex continues northward movement as stronger northward currents return to southern coastal areas.

reaching  $20 \text{ cm s}^{-1}$ . These mixed layer differences are common during time periods of relative low wind forcing as evident in the 10-m surface wind decrease to less than  $2 \text{ m s}^{-1}$  by 1 January 2005. Unassociated with this subtle mixed layer stratification was a subsurface signature below 50 m indicating a marked baroclinic structure (i.e., vertical shear). Surface current images on 29 December suggested a frontal eddy propagating into the HF radar domain (Figure 10a). The northward flowing FC was deflected  $\approx 10 \text{ km}$  offshore at 2000 GMT 29 December. On 30 December, the frontal eddy retracted shoreward and was elongated in the along-shelf direction, and by 0100 GMT 31 December, the FC axis shifted westward closer to its mean state as the eddy-like feature exited the region. Coastal surface current vectors neither indicated southward flows nor a circulation center for this observed frontal eddy. The cross-shelf velocity component reveals a

subsurface reversal that intensified with depth (Figure 9). The subsurface  $u$  and  $v$  components suggested weaker magnitudes with minor directional changes at 14-m depth whereas flows at 70-m depth were intense and toward the southwest. During this period, the  $u$  component surface velocities were  $-30 \text{ cm s}^{-1}$  at the cell nearest the ADCP mooring. Wind-driven currents, estimated following *Pond and Pickard* [1983], during this period were weak with values less than  $8 \text{ cm s}^{-1}$  for both components at the surface and 14-m depth. Differences in the wind-driven flows were  $\approx 5 \text{ cm s}^{-1}$  accounting for only 35% of the differences. This result suggests another forcing mechanism is responsible for the large cross-shelf differences in the upper 14 m of the water column. This period of low-correlation indices and flow structure underscores the importance of concurrent oceanographic measurements at and below the surface.

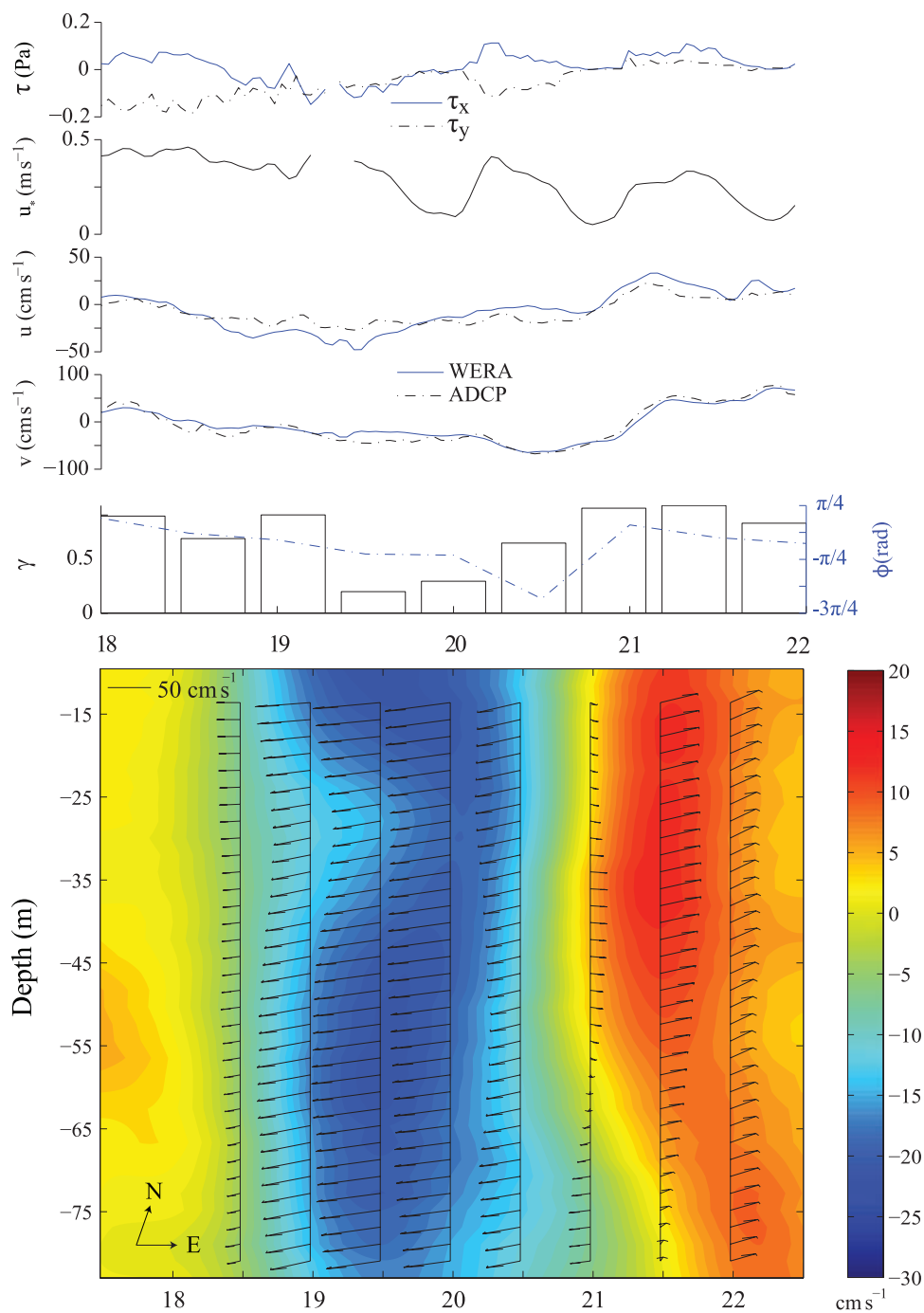


**Figure 12.** Time series analysis from 18 to 22 January 2005. Same as Figure 9.

#### 4.2. Submesoscale Vortex

[23] A submesoscale coherent vortex with a horizontal extent of  $\approx 15$  km was observed from 18 to 21 January 2005 (YD 18–21) within the radar domain (Figure 11). For the purpose of this study, submesoscale refers to features with length scales less than the internal deformation radius (approximately 30 km for the SOF). Two days prior to this event, a strong cold front moved through the South Florida region. The 10-m surface winds at Fowey Rocks were greater than  $10 \text{ m s}^{-1}$  from the NW (Figure 12, top). Surface frictional velocities ( $u_*$ ) during this time period

were greater than  $0.5 \text{ m s}^{-1}$ . This strong atmospheric forcing created a coastal countercurrent flowing southward along the inshore of the continental shelf break. During 18–21 January, the wind weakened and veered toward the SW. This forcing appears to coincide with the development of a submesoscale vortex centered along the shelf break. Surface current imagery (see Figure 11) shows the feature shoreward of the northward flowing FC. From the images, the genesis of this feature induced a subtle shift in the FC near the shelf break of  $\approx 1$  km. On 0000 GMT 21 January, the submesoscale feature moved downstream as the winds

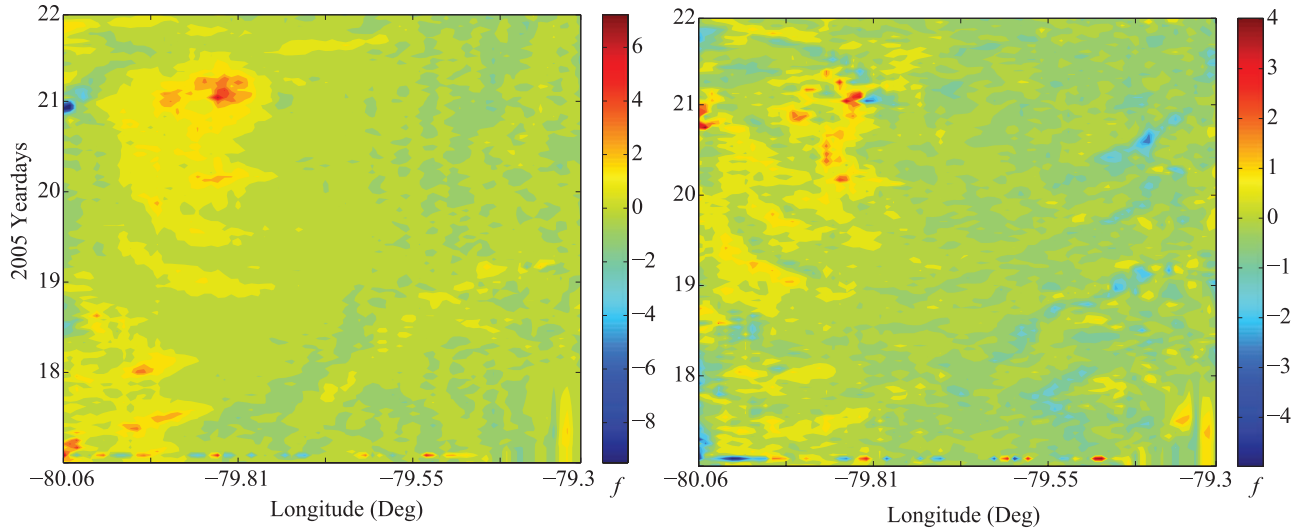


**Figure 13.** (left) Vorticity normalized by the Coriolis force across the Florida Straits from 17 to 22 January 2005. Positive vorticity (red) indicates cyclonic motion. (right) Normalized divergence during the same time period. Positive divergence (red) indicates upwelling due to the vortex.

relaxed and veered to the SW. As shown in Figure 13 (left), a spatial context to this downstream propagating vortex is given over an approximate 5-day time period. The feature was eventually sheared by FC interactions at 1500 GMT 21 January. Using surface current vectors, the translational velocity of this feature was  $\approx 45 \text{ cm s}^{-1}$ , slightly greater than the  $30 \text{ cm s}^{-1}$  found in previous studies [Shay *et al.*, 1998, 2000]. This event was also observed at the ADCP mooring where profiles had barotropic current structure suggestive of cross-shelf exchange persisting over a 3-day period (Figure 12, bottom). Cross- and along-shelf surface currents reached a minimum of  $-47$  and  $-65 \text{ cm s}^{-1}$ , respectively, during this time. Estimated cross- and along-shelf wind-driven currents ranged from  $-12$  to  $12 \text{ cm s}^{-1}$  and  $-12$  to  $3 \text{ cm s}^{-1}$  at the surface, respectively [Pond and Pickard, 1983]. The amplitude of wind-driven current components accounts for  $\approx 40\%$  and  $\approx 8\%$  of the observed surface and subsurface cross-shelf currents over this period. Surface current reversals on 20 January coincides with the shift in wind-driven velocity components. These results suggest that while profoundly affecting the observed cross-shelf velocity component, wind forcing alone does not account for the current structure observed during this event in agreement with the analysis of longer-term records [Parks, 2008].

[24] To estimate vorticity and divergence fields during this event, data along three adjacent transects of surface current measurements (25.4784, 25.4874 and 25.4964) were utilized. Initially, these data sets contained 20-min sample intervals. Small gaps in this data were linearly interpolated across along the time dimension then averaged on an hourly basis. The equation for vorticity normalized by local Coriolis  $f$  is given by

$$\zeta = \frac{1}{f} \left( \frac{\partial v}{\partial x} - \frac{\partial u}{\partial y} \right), \quad (4)$$

while the equation for normalized divergence is

$$\text{Div} = \frac{1}{f} \left( \frac{\partial u}{\partial x} + \frac{\partial v}{\partial y} \right). \quad (5)$$

These calculations were estimated at 2.4 km resolution using a centered difference method following Haltiner and Williams [1980]. The local vorticities, normalized by the local Coriolis parameter  $f$ , associated with the propagating submesoscale vortex were on the order of 5 to  $7f$  (Figure 13). This result is consistent with previous findings in the SOF [Peters *et al.*, 2002]. The associate divergence along this transect peaked at the same time, 0000 GMT 21 January, at approximately 3 to  $4f$  and presumably induced upwelling in that regime.

### 4.3. Mesoscale Eddy

[25] The third feature was a mesoscale eddy event observed in the surface current imagery from 17 to 21 February 2005 (YD 48–52). During this period, winds were relatively calm at Fowey Rocks prior to this event, less than  $2 \text{ m s}^{-1}$ . This event was observed at a time with large curvature in the FC axis in both surface current (Figure 14) and Moderate Resolution Imaging Spectroradiometer (MODIS) imagery. From MODIS, the image observed can be identified as the downstream expression of a propagating Tortugas Gyre, a semipermanent feature generated where the Loop Current enters the SOF [Fratantoni *et al.*, 1998]. The along-shelf component velocity began to weaken as the feature entered the radar domain on 17 February (YD 48). As the feature persisted,  $v$  velocities became near zero while surface  $u$  component velocities were shoreward and slightly stronger than the subsurface currents at 14-m depth (Figure 15). Current reversals were observed at the ADCP mooring with slight intensification of cross-shelf flow with depth between 14 and 35 m. In comparison to the submesoscale event, velocities were not

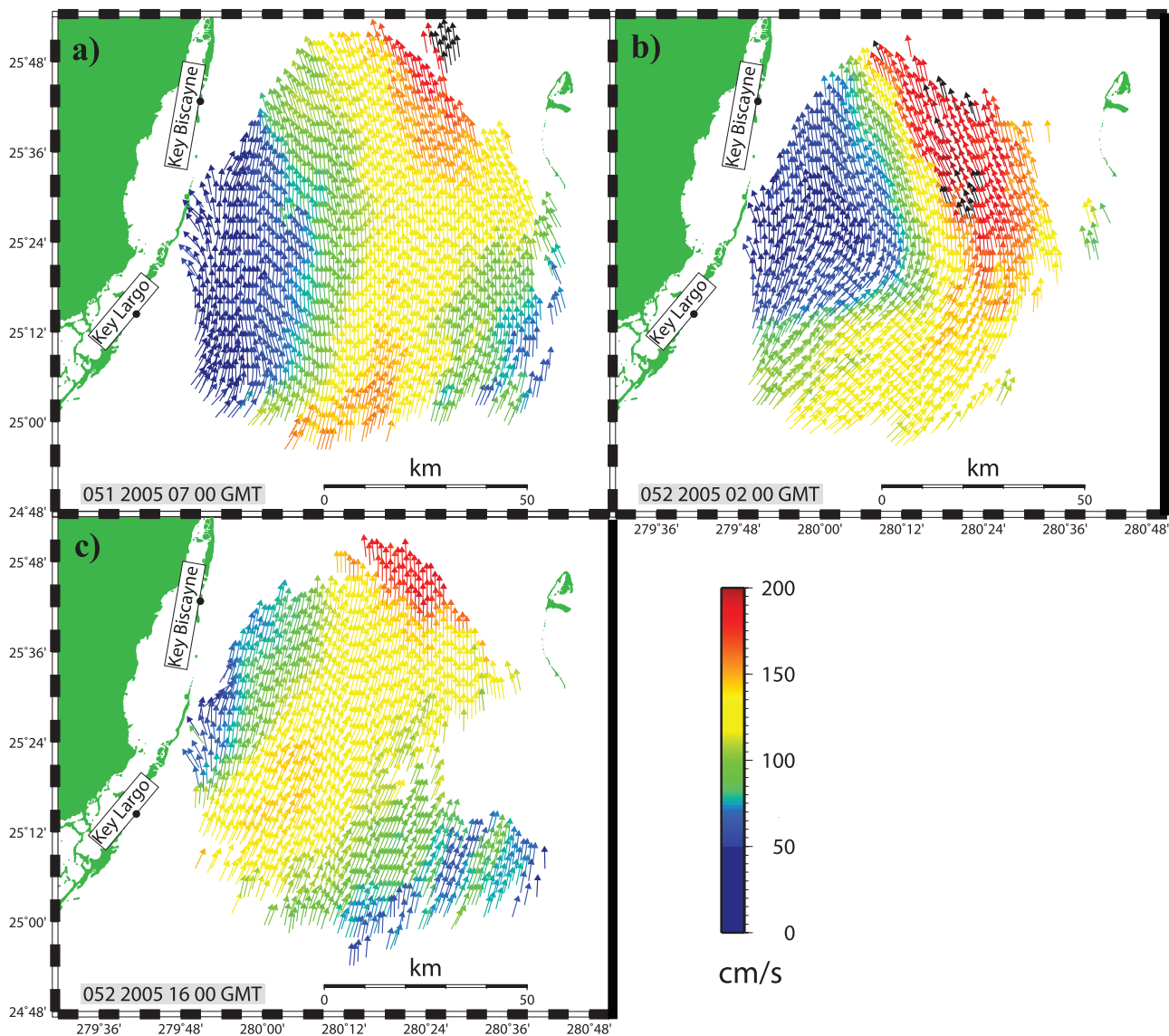


**Figure 14.** Hourly averaged WERA surface current observations on a 2.4-km grid showing the response to forcing from a mesoscale feature (propagating Tortugas Gyre). (a) Axis of FC moves shoreward as weak coastal currents continue. (b) FC intensification; mesoscale surface feature exhibited by strong curvature of surface current propagating north. (c) Mesoscale feature leaves domain as FC axis continues to return to mean position.

as intense with stratification in the mixed layer. This event persisted in the radar domain for approximately 3 days. At 0000 GMT 21 February, the FC showed intensification as its curvature around the mesoscale feature peaked. Current vector velocities reached magnitudes greater than  $2 \text{ m s}^{-1}$  at this time. Later on 1600 GMT 21 February, the FC relaxed and resembled a flow closer to its mean state (see Figure 8a) as the feature propagated north out of the radar domain.

## 5. Summary and Concluding Remarks

[26] The coastal ocean in South Florida consists of processes occurring over a spectrum of spatial and temporal scales. Difficulties in observing spectrum of small-scale processes are exacerbated in a region influenced by a western boundary current (i.e., Florida Current). Higher-resolution HF radars

allow for observations of ocean features embedded in the FC. Transmitting at 16.045 MHz, a dual-station high-frequency radar was deployed along the EFS and operated throughout a 9-month ADCP deployment. In a 16-element phased array mode, this HF radar mapped coastal currents at one kilometer resolution over an approximate  $50 \text{ km} \times 100 \text{ km}$  footprint. For comparison, concurrent subsurface measurements were obtained by a broadband ADCP along the shelf break within the radar domain. RMS differences ranged from  $0.1$  to  $0.3 \text{ m s}^{-1}$  between the surface and subsurface current measurements at 14-m depth suggestive of good quality data. Regression analyses indicate slopes near unity for the  $v$  component velocity throughout the deployment. By contrast, slopes for the  $u$  component velocity were  $\leq 0.5$  due to the variability in the region dominated by smaller-scale processes.

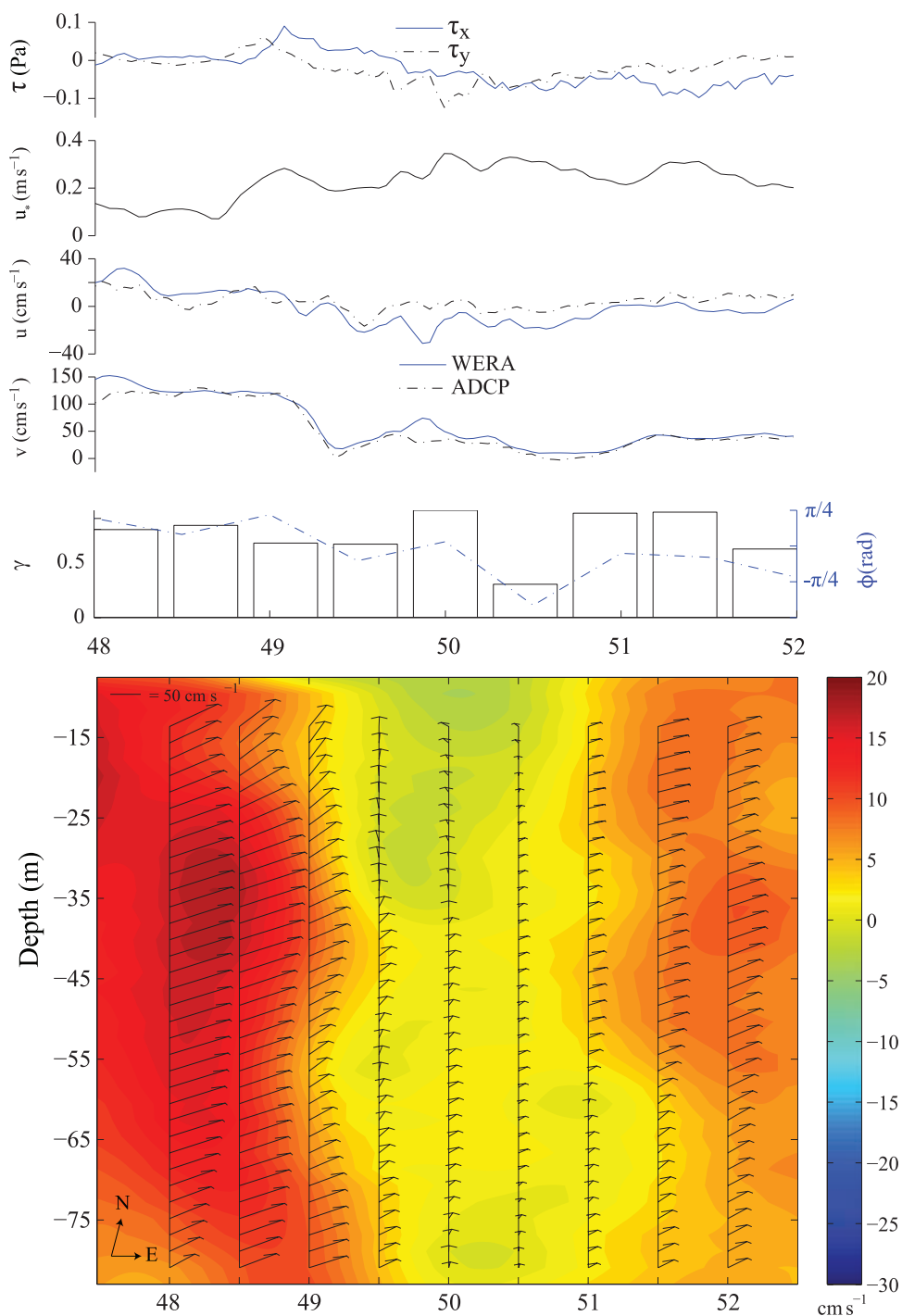


**Figure 15.** Time series analysis from 18 to 22 February 2005 (YD 48–52). Same as Figure 9.

[27] Current reversals were observed in the both sets of measurements during the deployment period. The surface current mapping system provides insight into the horizontal structure over a spectrum of FC variations. When used in tandem with other in situ sensors, three-dimensional snapshots can provide a better understanding of the kinematical structure of ocean features with depth. In this paper, three such interesting phenomena were discussed. A frontal eddy moved into the HF radar domain that induced a deflection in the FC axis of several kilometers. Inshore of the FC axis, surface current velocities were westward and not well

correlated with those observed at 14-m depth. Current profiler measurements indicated a low-velocity layer down to 70-m depth. Below this layer, velocity vectors suggest a southwestward countercurrent near the shelf break ocean bottom. An atmospheric cold front and associated wind forcing created a countercurrent and subsequent submeso-scale vortex that interacted with the northward flowing FC. Normalized vorticities associated with this feature peaked around  $5f$ , consistent with prior findings [Peters *et al.*, 2002]. A propagating Tortugas gyre, a common feature in the region, was observed in the radar domain and persisted

for 3 days. When the FC axis curvature was at its maximum during this time, flows in the FC core were greater than  $2 \text{ m s}^{-1}$ . These are examples of numerous other submesoscale and mesoscale features observed over the duration of the WERA record. Utilizing the entire HF radar domain enables estimates of translational speeds of coastal oceanographic features. Additionally, the periodicity of such features and the resulting time for FC adjustment can be assessed. The surface velocity data has shown high horizontal shears to develop over short time intervals associated with FC variability. Ultimately, these measurements are being used to test parameterizations used in coastal ocean models with the aim of resolving smaller-scale processes. By utilizing concurrent measurements, advancements can be made in understanding the dynamics behind complex, small-scale oceanographic features [Shay et al., 2000].

[28] **Acknowledgments.** The authors gratefully acknowledge the support by the ONR through SEA-COOS program (N00014-02-1-0972) administered by the University of North Carolina at Chapel Hill and the NOAA IOOS-supported Southeast Coastal Ocean Observing Regional Association through grants (NA08NOS47304094 and NA05NOS4261154). Brad Parks appreciates a graduate student research stipend provided by Stanford Caribbean Investments, LLC. We are thankful for the continued efforts of Brian Haus and Jodi Brewster of the Rosenstiel School of Marine and Atmospheric Science. We thank Renate Skinner, Jim Duquesnel, and Eric Kiefer of the Department of Environmental Protection, Florida Park Service for our site at the Key Largo Botanical Preserve; Kevin Kirwan, Michael McCaffery, and Ernest Lynk of the Miami Dade County Parks and Recreation for our site in Crandon Park; and Ramon Alfonso and his facilities staff for assisting us with the deployment at Crandon Park.

## References

- Broche, P., M. Crochet, J. C. Demaistre, J. L. Devenon, and P. Forget (1987), VHF radar for ocean surface current and sea state remote sensing, *Radio Sci.*, **22**, 69–75.
- Chapman, R. D., L. K. Shay, H. C. Graber, J. B. Edson, A. Karachintsev, C. L. Trump, and D. B. Ross (1997), On the accuracy of HF radar surface current measurements: Intercomparisons with ship-based sensors, *J. Geophys. Res.*, **102**(C8), 18,737–18,748.
- Crombie, D. D. (1955), Doppler spectrum of sea echo at 13.56 Mc/s, *Nature*, **175**, 681–682.
- Essen, H.-H., K.-W. Gurgel, and T. Schlick (2000), On the accuracy of current measurements by means of HF radar, *IEEE J. Oceanic Eng.*, **25**, 472–480.
- Fairall, C. W., E. F. Bradley, D. P. Rogers, J. B. Edson, and G. S. Young (1996), Bulk parameterization of air-sea fluxes for the Tropical Ocean–Global Atmosphere Coupled-Ocean Atmosphere Response Experiment, *J. Geophys. Res.*, **101**(C2), 3747–3764.
- Fratantoni, P. S., T. N. Lee, G. P. Podesta, and F. Muller-Karger (1998), The influence of Loop Current perturbations on the formation and evolution of Tortugas eddies in the southern Straits of Florida, *J. Geophys. Res.*, **103**(C11), 24,759–24,799.
- Gurgel, K.-W. (1994), Shipborne measurement of surface current fields by HF radar, *Onde Electr.*, **74**(5), 54–59.
- Gurgel, K.-W., G. Antonischki, H.-H. Essen, and T. Schlick (1999a), Wellen radar (WERA): A new ground wave HF radar for remote sensing, *Coastal Eng.*, **37**, 219–234.
- Gurgel, K.-W., H.-H. Essen, and S. P. Kingsley (1999b), High frequency radars: Limitations and recent developments, *Coastal Eng.*, **37**, 201–218.
- Haltiner, G. J., and R. T. Williams (1980), Numerical methods in *Numerical Prediction and Dynamic Meteorology*, 2nd ed., chap. 5 pp. 108–109, John Wiley, New York.
- Hamilton, P., J. C. Larsen, K. D. Leaman, T. N. Lee, and E. Waddell (2005), Transports through the Straits of Florida, *J. Phys. Oceanogr.*, **35**, 308–322.
- Haus, B. K., J. D. Wang, J. Rivera, J. Martinez-Pedraja, and N. Smith (2000), Remote radar measurement of shelf currents of Key Largo, Florida, *Estuarine Coastal Shelf Sci.*, **51**, 553–569.
- Haus, B. K., J. D. Wang, J. Martinez-Pedraja, and N. Smith (2004), Southeast Florida Shelf circulation and volume exchange, observations of km-scale variability, *Estuarine Coastal Shelf Sci.*, **59**, 277–294.
- Kundu, P. K. (1976a), An analysis of inertial oscillations observed near Oregon coast, *J. Phys. Oceanogr.*, **6**, 879–893.
- Kundu, P. K. (1976b), Ekman veering near the ocean bottom, *J. Phys. Oceanogr.*, **6**, 238–242.
- Large, W. G., and S. Pond (1981), Open ocean momentum flux measurements in moderate to strong winds, *J. Phys. Oceanogr.*, **11**, 324–336.
- Lee, T. N., and D. A. Mayer (1977), Low-frequency variability and spin-off eddies along the shelf off southeast Florida, *J. Mar. Res.*, **35**, 193–220.
- Lee, T. N., C. Rooth, E. Williams, M. McGowan, A. F. Szamant, and M. E. Clarke (1992), Influence of Florida Current, gyres and wind-driven circulation on transport of larvae and recruitment in the Florida Keys coral reefs, *Cont. Shelf Res.*, **12**(7–8), 971–1002.
- Lee, T. N., K. D. Leaman, E. Williams, T. Berger, and L. Atkinson (1995), Florida Current meanders and gyre formation in the southern Straits of Florida, *J. Geophys. Res.*, **100**(C5), 8606–8620.
- Liu, Y., R. H. Weisberg, and L. K. Shay (2007), Current patterns on the West Florida Shelf from joint self-organizing map analyses of HF radar and ADCP data, *J. Atmos. Oceanic Technol.*, **24**(4), 702–712.
- Otnes, R. K., and L. Enochson (1978), *Applied Time Series Analysis: Basic Techniques* vol. 1, 449 pp. John Wiley, New York.
- Parks, A. B. (2008), Observing eddy variability using HF radar in the Straits of Florida, M.S. thesis, Univ. of Miami, Coral Gables, Fla.
- Peters, H., L. K. Shay, A. J. Mariano, and T. M. Cook (2002), Current variability on a narrow shelf with large ambient vorticity, *J. Geophys. Res.*, **107**(C8), 3087, doi:10.1029/2001JC000813.
- Pond, S., and G. L. Pickard (1983), Currents with friction: Wind-driven circulation, in *Introduction to Dynamical Oceanography*, 2nd ed., chap. 9, pp. 106–110, Butterworth-Heinemann, Oxford, U. K.
- Shay, L. K., H. C. Graber, D. B. Ross, and R. D. Chapman (1995), Mesoscale ocean surface current structure detected by high-frequency radar, *J. Atmos. Oceanic Technol.*, **12**(4), 881–900.
- Shay, L. K., T. N. Lee, E. J. Williams, H. C. Graber, and C. G. H. Rooth (1998), Effects of low-frequency current variability on near-inertial submesoscale vortices, *J. Geophys. Res.*, **103**(C9), 18,691–18,714.
- Shay, L. K., et al. (2000), VHF radar detects oceanic submesoscale vortex along Florida coast, *Eos Trans. AGU*, **81**(19), 209–213.
- Shay, L. K., T. M. Cook, H. Peters, A. J. Mariano, R. H. Weisberg, P. E. An, A. Soloviev, and M. Luther (2002), Very high-frequency radar mapping of surface currents, *IEEE J. Oceanic Eng.*, **27**, 155–169.
- Shay, L. K., J. Martinez, T. M. Cook, B. K. Haus, and R. H. Weisberg (2007), High frequency surface current mapping using Wellen radar, *J. Atmos. Oceanic Technol.*, **24**(3), 484–503.
- Shay, L. K., D. Savidge, R. Styles, H. Seim, and R. H. Weisberg (2008), High-frequency radar observing systems in SEACOOS, *Mar. Technol. Soc. J.*, **42**, 55–67.
- Stewart, R. H., and J. W. Joy (1974), HF radio measurements of ocean surface currents, *Deep Sea Res. Oceanogr. Abstr.*, **21**, 1039–1049.
- Teague, C. C., J. F. Vesceky, and Z. R. Hallock (2001), A comparison of multifrequency HF radar and ADCP measurements of near-surface currents during COPE-3, *IEEE J. Oceanic Eng.*, **26**, 399–405.

K.-W. Gurgel, Institute of Oceanography, Center for Marine and Climate Research, University of Hamburg, D-20146 Hamburg, Germany.

W. E. Johns, J. Martinez-Pedraja, and L. K. Shay, Division of Meteorology and Physical Oceanography, Rosenstiel School of Marine and Atmospheric Science, University of Miami, 4600 Rickenbacker Causeway, Miami, FL 33133, USA.

A. B. Parks, Integral Consulting, Inc., 4D Bay Street, Berlin, MD 21811, USA. (bparks@integral-corp.com)